AIP Journal of Applied Physics

Critical thickness for stripe domain formation in FePt thin films: Dependence on residual stress

N. R. Álvarez, J. E. Gómez, A. E. Moya Riffo, M. A. Vicente Álvarez, and A. Butera

Citation: Journal of Applied Physics **119**, 083906 (2016); doi: 10.1063/1.4942652
View online: http://dx.doi.org/10.1063/1.4942652
View Table of Contents: http://scitation.aip.org/content/aip/journal/jap/119/8?ver=pdfcov
Published by the AIP Publishing

Critical thickness for stripe domain formation in FePt thin films: Dependence on residual stress

N. R. Álvarez,[1] J. E. Gómez,[1] A. E. Moya Riffo,[1] M. A. Vicente Álvarez,[1] and A. Butera[2,a)]
[1]*Centro Atómico Bariloche (CNEA) and Conicet, 8400 Bariloche, Río Negro, Argentina*
[2]*Centro Atómico Bariloche (CNEA), Instituto Balseiro (U. N. Cuyo), and Conicet, 8400 Bariloche, Río Negro, Argentina*

(Received 23 October 2015; accepted 12 February 2016; published online 25 February 2016)

Magnetically soft FePt thin films of varying thickness ($20\,\text{nm} \leq d \leq 100\,\text{nm}$) were sputter-deposited at different Ar pressures in order to systematically modify the residual stress and hence the magnetic anisotropy. The magnetic domain structure of FePt thin films showed a transition from planar to nearly parallel stripes above a critical thickness, d_{cr}, which was found to depend on an anisotropy contribution perpendicular to the film plane, originated essentially in magnetoelastic effects. A careful structural characterization was made in order to obtain the strain and the stress induced magnetic anisotropy in the samples. Vibrating sample magnetometry and magnetic force microscopy were used to investigate the changes occurring in the magnetic domain structure and the critical thickness of each set of films. Joining together structural and magnetic results, we have been able to construct a phase diagram that divided regions of different domain structures, either by changing the film thickness or the perpendicular magnetic anisotropy. The experimental results could be satisfactorily explained by using a model developed by Murayama. The observed dependence of the magnetic properties of soft FePt thin films on the fabrication conditions opens the possibility to tune the magnetic domain configuration from planar to stripe-like domains by changing the argon sputtering pressure used during film deposition. © *2016 AIP Publishing LLC*.
[http://dx.doi.org/10.1063/1.4942652]

I. INTRODUCTION

Novel magnetoelectric devices, such as tunable microwave components, filters, attenuators, phase-shifters, or resonators,[1–3] can be designed by the smart combination of a ferromagnetic film with a piezoelectric substrate in order to control the magnetic anisotropy of the ferromagnet using electric fields. The ferromagnets needed for these applications should be magnetically soft and possess a large magnetostriction constant. Interest in soft Fe alloys (for example, FeGa, FeCo, FePt, and FePd) reappeared recently because of potential applications in magnetoelectrically coupled devices. In particular, FePt equiatomic alloy films have a relatively narrow ferromagnetic absorption line and a considerably large magnetostriction and saturation magnetization. These films can be sputtered on piezoelectric wafers, such as PMN-PT ($PbMg_{1/3}Nb_{2/3}O_3$-$PbTiO_3$), to display magnetoelectric couplings of several tens of Oe.cm/kV in the microwave region.[3] However, it was found that the magnetoelectric response was different in similar materials (see, for example, Refs. 3 and 4), which indicates the need to study and control in more detail the effects of different growing conditions on the initial magnetic state.

FePt thin films grown by sputtering techniques usually form in a chemically disordered phase (called A1) with relatively soft magnetic properties. These films show a critical thickness above which the magnetic domains change from a planar to a stripe-like configuration.[5] The stripe pattern is induced by a perpendicular magnetic anisotropy, called $K_\perp$, originated by the combined contributions of magneto-crystalline energy and magneto-elastic effects.[5]

The critical thickness above which the magnetic domain configuration changes from planar to stripe-like domains strongly depends on the ratio between $K_\perp$ and the demagnetizing energy. This ratio is known as the quality factor $Q = K_\perp/2\pi M_s^2$, being M_s the saturation magnetization of the material. As a general rule, if $Q > 1$, the perpendicular anisotropy is strong enough to align the magnetization normal to the film plane and if $Q < 1$, the competition between the two energies results in a magnetization that stays essentially in the film plane, but has an alternating component in the normal direction.[6] It is possible to modify $K_\perp$, and consequently Q, through the modification of the crystalline texture or the residual stress in the samples. Several authors have already shown that it is possible to control the residual stress of thin layers by varying the conditions of the thin film deposition process, in particular, the Ar pressure (P_{Ar}) inside the sputtering chamber.[7–10]

Different magnetic properties of FePt single layers fabricated with the same growing conditions have been previously characterized by our group as a function of film thickness. In particular, we have studied the changes in the domain configuration,[5,11] the effects of temperature on the magnetic structure,[12,13] the dynamical response,[14–16] and the presence of standing spin waves.[17] There are also studies in which the film thickness remains fixed and the residual stress is changed by modifying the growing conditions.[7,10] In this work, we report a detailed investigation of the structural

a)Also at INN - Instituto de Nanociencia y Nanotecnología, Argentina. Electronic mail: butera@cab.cnea.gov.ar.

properties of the FePt system for samples in which the growing conditions and the film thickness are systematically changed, and correlate these results with the critical thickness for the transition from planar magnetic domains to a stripe-like configuration. The possibility of tuning the initial strain of the films allowed us to study this transition as a function of stress for samples in a defined range of film thicknesses. The experimental data were then used to construct a phase diagram that correlates the quality factor Q with the critical thickness.

II. EXPERIMENTAL DETAILS

The samples were grown by dc magnetron sputtering techniques on naturally oxidized Si (100) substrates from a target with a measured Fe:Pt atomic composition 45:55. As we wanted to fully characterize the transition occurring in the magnetic domain structure, we prepared different sets of samples in which either the film thickness (d) or the sputtering P_{Ar} was systematically changed. In the first batch of six samples (called batch A), we varied P_{Ar} in the chamber in the range 3–13 mTorr while maintaining a constant thickness $d = 100$ nm. Previous studies of the magnetic properties of these films showed a transition from stripe-like to in-plane magnetic domains for P_{Ar} between 9 and 11 mTorr.[7,10] It is worth mentioning that this transition is not abrupt, but the samples close to the critical pressure P_{Ar} exhibit some characteristic features of both systems.

Knowing the critical value of P_{Ar} for a given thickness, and with the aim of studying this transition for different pressures, a second batch (B) consisting of three series of samples with constant P_{Ar} and varying d was grown. Since we already performed an extensive study in samples sputtered with $P_{Ar} = 3$ mTorr,[5,17] we fabricated new series with $P_{Ar} = 5$ mTorr and thicknesses $d = 20$, 31, 40, 47, 63 nm (batch B1); $P_{Ar} = 7$ mTorr and $d = 51$, 56, 73, 81, 89 nm (batch B2); and $P_{Ar} = 9$ mTorr and $d = 71$, 78, 82, 94, 99 nm (batch B3). Table I summarizes the growing conditions and the film thickness of the 21 samples studied in this work. The thickness range for each sputtering pressure was chosen expecting to include the critical thickness in which the magnetic domain structure should change. In order to protect the films from oxidation, a thin capping layer of approximately 3 nm of a non-magnetic material (Pt for batch A and Ru for batches B1-B3) was grown on top of each sample. Additional details about the fabrication process can be found in Refs. 5 and 14.

TABLE I. Detail of the different sets of samples studied in this work.

Batch A $d = 100$ nm P_{Ar} (mTorr)	Batch B1 $P_{Ar} = 5$ mTorr d (nm)	Batch B2 $P_{Ar} = 7$ mTorr d (nm)	Batch B3 $P_{Ar} = 9$ mTorr d (nm)
3	20	51	71
5	31	56	78
7	40	73	82
9	47	81	94
11	63	89	99
13	…	…	…

The structure, texture, and residual stress of the films were characterized using X-ray diffractometry in a PANalytical Empyrean diffractometer equipped with a Cu X-ray tube ($\lambda K_{\alpha}Cu = 0.15418$ nm). We performed conventional Bragg-Brentano θ–2θ scans (2θ is the angle between the incident and the diffracted beams) for the determination of the interplanar distances d_{hkl} and ψ scans for strain/stress studies. Pole figures of selected samples were obtained in the same system using an Eulerian Cradle designed for texture analysis. For a better alignment of the samples, the diffractograms were acquired by performing a previous rocking curve around the (004) diffraction peak of the Si substrate.

A Vibrating Sample Magnetometer (VSM - Lakeshore 7404) was used to investigate the magnetic behavior of the samples as a function of magnetic field at room temperature. Hysteresis loops were acquired with the external field parallel and perpendicular to the film plane. The surface topography and the magnetic domain structure investigations were carried out using a Magnetic Force Microscope (AFM/MFM Veeco Dimension 3100 with Nanoscope IV electronics). The microscope was operated in the tapping/lift mode, which allows both the topographic and the magnetic force image to be collected simultaneously in the same scan area. Medium moment-medium coercivity tips from Bruker (MESP) were magnetized along the direction of the tip, so the images taken show the stray field gradient in the direction perpendicular to the film plane.

III. RESULTS AND DISCUSSION

A. Microstructural characterization

The X-ray diffraction data acquired for different films showed that, in general, the main characteristics of the diffractograms, such as texture, grain size, and residual stress, tend to vary with the Ar pressure of each batch (see Figs. 1(a) and 1(b)) but do not change significantly with the thickness, as can be seen in inset of Fig. 1.

The absence of superlattice peaks in the diffraction patterns and also the soft magnetic properties of the films (that will be presented in Sec. III B) indicate that all samples have grown in the A1 crystalline phase and are strongly textured in the [111] direction. In the range $30° \leq 2\theta \leq 70°$, the only diffraction peaks from the FePt layer that can be observed are the (111) and (200). The FePt (220) peak, expected at $2\theta \sim 69.7°$, is overlapped with the much more intense (400) diffraction corresponding to the Si substrate. The (311) and (222) FePt reflections (not shown in Fig. 1) can be observed for $2\theta \gtrsim 83°$. The degree of crystalline texture can be estimated from the comparison between the ratio of the areas of the diffraction peaks $I(111)/I(200)$ which is a good indication of the preferential orientation of the grains in the [111] direction. We have found that this ratio does not vary significantly with the thickness in the range $10\,\text{nm} < d < 100\,\text{nm}$ ($I(111)/I(200) \sim 10$ for $P_{Ar} = 3$ mTorr), but when the Ar pressure is increased, the ratio between the intensities of the FePt diffraction peaks increases systematically reaching $I(111)/I(200) \sim 25$ for $P_{Ar} = 13$ mTorr. As a reference, the intensity ratio for a collection of randomly oriented grains should be $I(111)/I(200) \sim 2$.

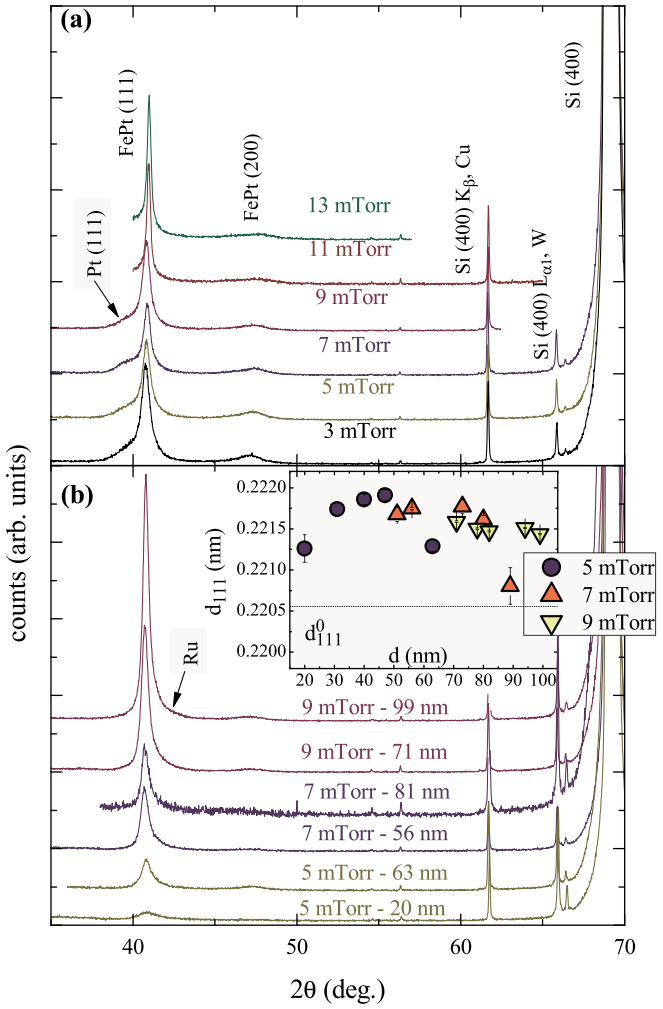

FIG. 1. X-ray diffraction patterns of typical FePt thin films grown at different Ar pressures. The top panel (a) corresponds to the samples of batch A, and panel (b) shows selected samples from batches B1–B3. As can be seen in the figures, it is possible to index the two FePt peaks in the range $30° \leq 2\theta \leq 70°$ as corresponding to the chemically disordered A1 phase. A peak of small intensity from either the Pt or the Ru capping layer can be also observed in panels (a) and (b), respectively. The inset shows the variation of the d_{111} interplanar distance for the different samples, where we have indicated with a horizontal line the relaxed d^0_{111} interplanar distance estimated from Fig. 4.

As we have mentioned above, a potential contribution to the perpendicular magnetic anisotropy could be due to the magnetocrystalline anisotropy. For a collection of randomly oriented grains this term averages zero, but if there is a preferential orientation of the crystalline grains a non-zero contribution could occur for certain textures. For the A1 phase, the [111] direction is an axis of easy magnetization[18] and the [111] texture observed in our films can then favor a magnetocrystalline contribution to the perpendicular anisotropy. Note also that a [111] texture is expected in relaxed fcc metallic films because it minimizes the energy associated with the interfaces (the top interface in contact with Pt or Ru and the bottom one in contact with the amorphous substrate) when the (111) planes of the crystalline grains are parallel to the surface.[9] This fact indicates the need to further characterize the film texture, for example, through the measurement of pole figures. In the Schulz method,[19,20] a texture goniometer is used. The 2θ angle is fixed for each polar figure, so one family of planes is analyzed, and the sample is rotated according to the two polar angles, the radial χ and the azimuthal ϕ (see Fig. 2 for the definition of the different angles used for texture and stress analysis).

In Figs. 3(a), 3(c), and 3(d), we present different pole figures measured in the sample FePt 100 nm–3 mTorr for the diffraction peaks (111), (200), and (311), observable at $2\theta \sim 41°$, 48°, and 84°, respectively, and a detail of the region close to $\chi = 0°$ for the (111) pole (Fig. 3(e)). Each point in the pole figure is the stereographic projection of the corresponding pole. We also show the simulated orientation distribution function (ODF) for a sample with a [111] fiber texture in Fig. 3(b). From the experimental data, it is possible to see that, as expected, the [111] direction has a very high intensity between $\chi = 0°$ and $\chi = 3°$ and then decreases, giving us an indication of a preferential orientation of the grains, close to the film plane normal. For $\chi \sim 70°$, the intensity rises again, consistent with the diffraction of different planes from the {111} family. An almost uniform distribution is observed for the angle ϕ, indicating the absence of preferential grain orientations in the film plane. This behavior correlates very well with the simulated ODF for a [111] fiber texture. The FePt (200) and (311) reflections are also observed at zero angle, indicating that a certain amount of grains have these axes perpendicular to the film plane, but they are much less intense than the FePt (111) reflection. In the pole figure of FePt (200) ($2\theta_{\mathrm{FePt(200)}} \sim 47.6°$), we can also identify the reflections of the Si substrate $2\theta_{\mathrm{Si(220)}} \sim 47.3°$. Note that the contributions of the film and the substrate can be easily distinguished, given that the latter is a single crystal and is represented by very intense discrete points in the figure and, on the other hand, the polycrystalline nature of the films gives rise to a ring. In order to calculate the distribution function, it is necessary to have pole figures of four different reflections, but since the sample is strongly textured the intensity of the reflections (200), (311), and (220) (which was also measured but not presented) is very small and this estimation could not be accomplished. Nevertheless, Fig. 3 shows that the grains are mostly oriented with the [111] axes normal to the film (with a dispersion of ~5°) and uniformly distributed in the film plane.

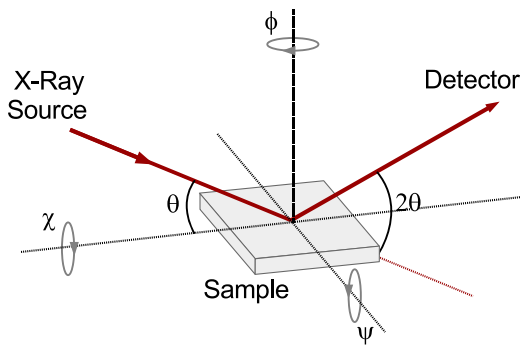

FIG. 2. Geometry for texture and stress measurements. In the first case, 2θ remains fixed at the maximum intensity of a given reflection, and for every χ step of 1° ($0° \leq \chi \leq 75°$), a 360° sweep in ϕ is performed (also in steps of 1°). For a stress measurement, $\chi = 0°$ is fixed and a conventional θ–2θ scan is acquired for discrete steps of the tilt angle ψ.

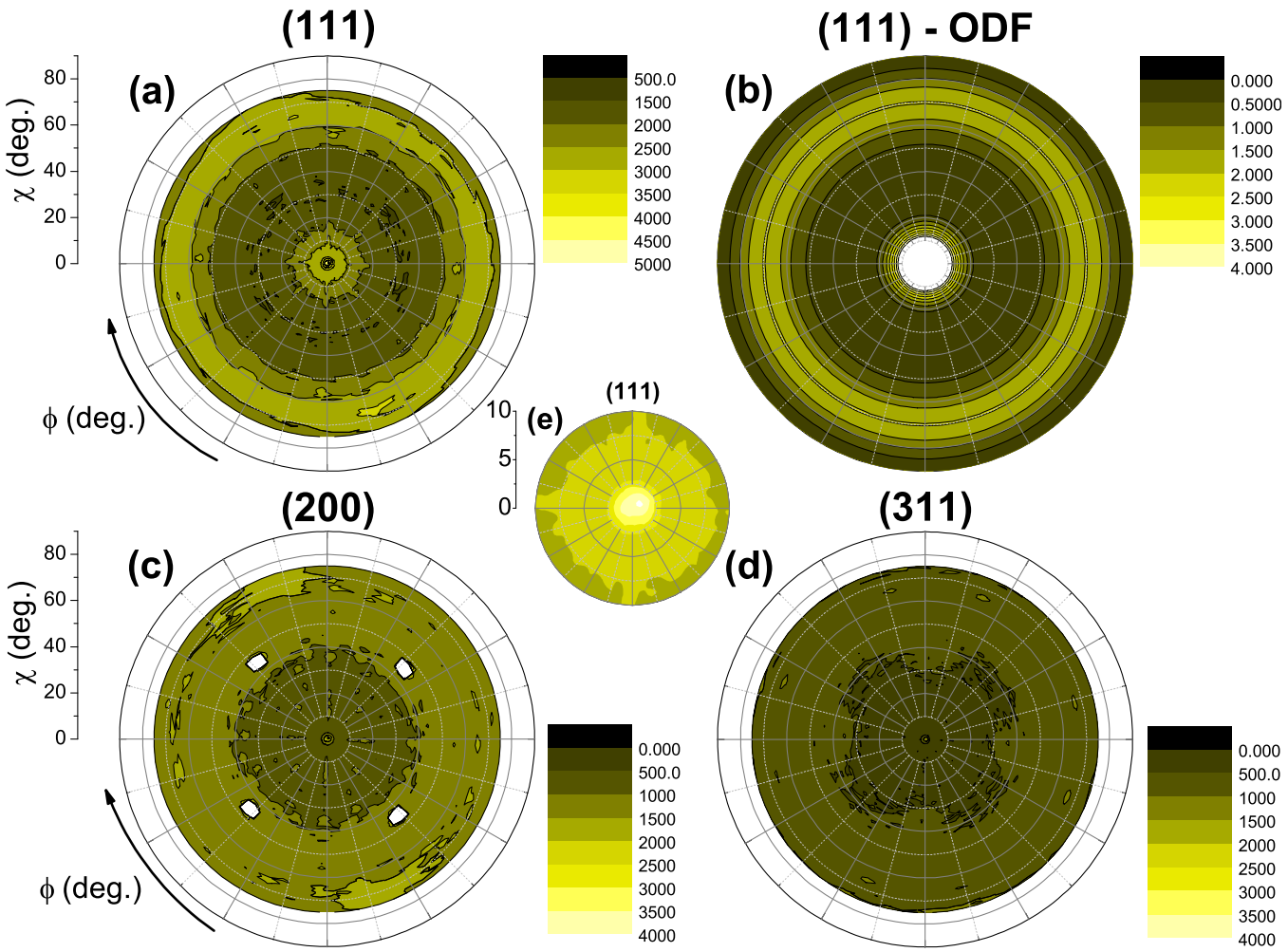

FIG. 3. Pole figures for FePt 100 nm–3 mTorr. From left to right, top to bottom, the figures correspond to (111) (a), simulated (111) ODF (b), (200) (c), and (311) (d) planes. No significant in-plane crystalline texture is observed. Panel (e) is a detail of the central region of the (111) pole figure. The bright spots in the (200) pole figure are due to the {220} family of reflections from the Si substrate.

Strain-stress studies were also performed in some selected samples of batch A ($P_{Ar} = 3$, 5, and 13 mTorr). In Fig. 4(a), we present θ–2θ X-ray diffractograms of the (311) reflection for the FePt 100 nm–3 mTorr film, measured for different tilt angles ψ. We studied this particular reflection because the high 2θ angles allowed us to use larger tilt values. As the position of the peak is in higher angles, its intensity decreases and it was necessary to use relatively larger collection times to determine the reflection angle and the interplanar distances d_{hkl} with a small error. We have found approximately the same d_{hkl} vs. $\sin^2\psi$ dependence for positive and negative values of the angle ψ. This absence of the so-called ψ-splitting[21] is indicating a nearly zero contribution of shear strains perpendicular to the film surface. In this case, a linear d_{311} vs. $\sin^2\psi$ behavior should be observed and the strain in the z-direction (ε_{33}) for given values of ϕ and the tilt angle ψ can be obtained from the following equation:[22]

$$\frac{d_{311}^{\phi\psi} - d_{311}^{0}}{d_{311}^{0}} = (\varepsilon_{11}\cos^2\phi + \varepsilon_{12}\cos 2\phi + \varepsilon_{22}\sin^2\phi - \varepsilon_{33})\sin^2\psi + \varepsilon_{33}, \quad (1)$$

where ε_{ij} are the strain components and d_{311}^{0} is the unstressed value for the interplanar (311) spacing. The index "33" indicates a direction perpendicular to the film plane, and "11" and "22" refer to orthogonal axes contained in the film plane.

The application of Eq. (1) requires the knowledge of the d_{311}^{0} value. This lattice spacing can be initially estimated by assuming that there are no shear stresses ($\varepsilon_{12} = 0$) and that the samples are isotropic in the film plane ($\varepsilon_{11} = \varepsilon_{22}$). This simplification for the estimation of d_{311}^{0} is based on the fact that the pole figures did not show a measurable in-plane anisotropy. In this situation, the ϕ dependence in Eq. (1) vanishes and the following expression holds:

$$d_{311}^{\phi\psi} \approx (\varepsilon_{11} - \varepsilon_{33})d_{311}^{0}\sin^2\psi + (\varepsilon_{33} + 1)d_{311}^{0} = -\frac{\nu + 1}{2\nu}\varepsilon_{33}d_{311}^{0}\sin^2\psi + (\varepsilon_{33} + 1)d_{311}^{0}. \quad (2)$$

In the above equation, ν is the Poisson's ratio that relates the strain in orthogonal directions. Since a uniform thin film is free to expand or contract in the direction normal to the film plane, the stress in the z-direction and the shear stresses that involve a component in this direction are zero.[23]

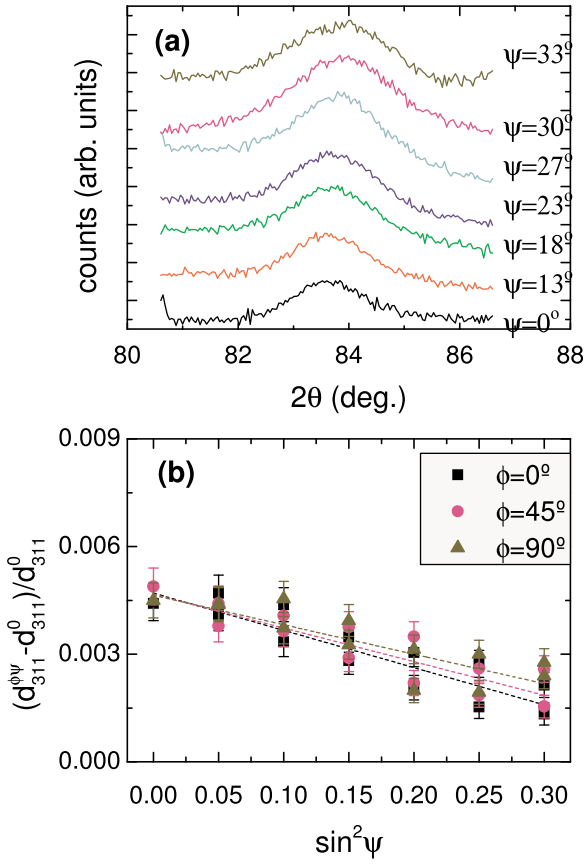

FIG. 4. (a) X-ray diffractograms for the (311) reflection in an FePt 100 nm−3 mTorr sample, varying the tilt angle ψ of the sample holder. (b) Parameter $d^{\phi\psi}_{311}/d^0_{311} - 1$ vs $\sin^2\psi$ (Eq. (1)) obtained from the X-ray scan for three different orientations of the angle ϕ. Dashed lines correspond to linear fits of the experimental data.

With these considerations, the equations of elasticity in the case of biaxial stress[22] take the following form:

$$\begin{aligned}\varepsilon_{11} &= \frac{1}{E}(\sigma_{11} - \nu\sigma_{22})\\ \varepsilon_{22} &= \frac{1}{E}(\sigma_{22} - \nu\sigma_{11})\\ \varepsilon_{33} &= -\frac{\nu}{E}(\sigma_{11} + \nu\sigma_{22})\\ \varepsilon_{12} &= \frac{1+\nu}{E}\sigma_{12},\end{aligned} \tag{3}$$

with E being the average Young's modulus and σ_{ij} the in-plane stresses in the directions $\hat{x}$ and $\hat{y}$ in the reference system of the sample. The Young's modulus of FePt thin films in the disordered A1 phase has not been directly measured to our knowledge. In a previous paper,[13] we measured the elasticity of bulk FePt in the ordered $L1_0$ phase, obtained with the vibrating reed technique in a rectangular shaped piece of the target used to grow the films. From the measured value, we estimated $E_{\text{FePt-A1}} = 130(10)$ GPa at room temperature for the disordered A1 phase.

For the evaluation of the strain, we used as an initial estimate the reported[7,24,25] value for the Poisson's ratio, $\nu_{\text{FePt}} = 0.33$. As we will show later, this consideration is in very good agreement with our final results. A value of the relaxed lattice parameter d^0_{311} can be then obtained from a linear fit of the data $d^{\phi\psi}_{311}$ vs. $\sin^2\psi$ (Eq. (2)) for each of the 3, 5, and 13 mTorr–100 nm samples. With this initial estimate for d^0_{311}, it is possible to fit $\frac{d^{\phi\psi}_{311} - d^0_{311}}{d^0_{311}}$ vs. $\sin^2\psi$ using Eq. (1) to calculate all the unknown strains ε_{ij}. The strain ε_{33} in the z-direction can be obtained from the average ordinate, and ε_{11}, ε_{22}, and the shear strain ε_{12}, from the slopes. Note that now we are not forcing the approximations of isotropy ($\varepsilon_{12} = 0$ and $\varepsilon_{11} = \varepsilon_{22}$) used for the initial estimation of d^0_{311}. In Fig. 4(b), we present the experimental data and the corresponding linear fits for the angles $\phi = 0^o$, 45°, and 90°.

The set of Eqs. (3) consists of four equations with four unknown parameters, three σ_{ij} and ν. With the new estimated value of ν, we can apply an iterative process and go back to Eq. (1) to calculate a new value of d^0_{311} and start the process again. We ended the iterations when the Poisson's ratio value was within the error of the last iteration.

In Fig. 5, we present the obtained stress values for the different films. We have found that the samples are compressed in the film plane and expanded in the normal direction for low values of P_{Ar} and change to the opposite behavior for $P_{\text{Ar}} = 13$ mTorr. Also, the shear stress σ_{12} is one order of magnitude smaller than the planar stresses σ_{11} and σ_{22}, again in agreement with the initial approximations.

Using the values obtained for three of the 100 nm samples ($P_{\text{Ar}} = 3$, 5, and 13 mTorr), we calculated an average value $\nu_{\text{FePt}} = 0.34(3)$ for the Poisson's ratio for FePt films in the crystalline disordered A1 phase, in very good agreement with the initial value $\nu_{\text{FePt}} = 0.33$ used in the first estimation of d^0_{311}. For the interplanar distance, we estimated a value $d^0_{311} = 0.11519(5)$ nm.

Because $\sin^2\psi$ experiments are very time consuming, we only performed these measurements on three representative samples. The overall behavior shows, as expected, a change to a tensile regime, which is fully developed for the 13 mTorr film.

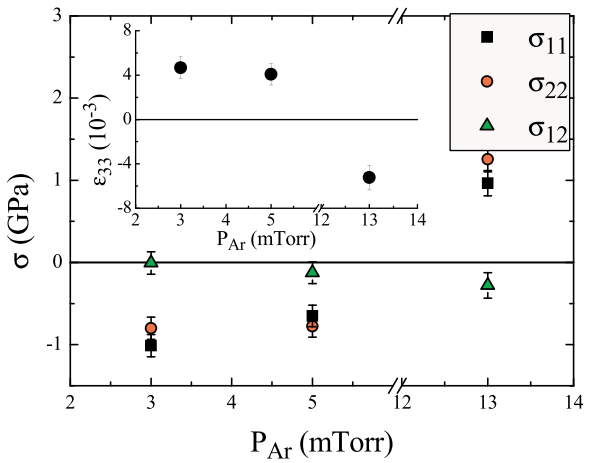

FIG. 5. In-plane residual stress as a function of Ar pressure for 100 nm films. The samples are mostly isotropic and under compressive stress at low P_{Ar} and change to tensile stress with increasing P_{Ar}. The directions 11 and 22 are arbitrary, according to the relative position of the film in the sample holder and the X-ray source. The inset shows the deformation in the perpendicular direction, ε_{33}, evidencing the change of the strain regime. All strain calculations were performed using the (311) reflection and the $\sin^2\psi$ method.

The results we have found in disordered FePt thin films agree well with other reports in metallic thin films,[26–28] in particular, FePt,[10,29] which show that a variation in P_{Ar} changes the surface morphology because more bombardment of the films (resputtering) occurs under higher pressure conditions. The atoms sputtered at low argon pressures have a higher surface mobility on the substrate, promoting the formation of denser films under compressive stress. When P_{Ar} is increased, the number of collisions of the sputtered and reflected atoms rises, lowering the mobility of the atoms on the substrate. This can have a significant effect on the growth kinetics of the depositing film. The increase in the scattering rate may also cause atoms to arrive to the substrate at oblique angles[30] resulting in a self-shadowing effect of the incident atoms by those already incorporated, and giving rise to a columnar growth,[31] enhancing the texture, and reducing the stress.

B. Magnetization and magnetic force microscopy measurements

The average saturation magnetization for the samples was obtained from the data of Fig. 6 resulting in $M_s = 930 \pm 20\,\text{emu/cm}^3$, somewhat smaller than the reported[32] bulk-value $M_s(\text{FePt}) \sim 1130\,\text{emu/cm}^3$. This difference, often reported in metallic thin films, may be explained by the small Pt off-stoichiometry of the sputtering target, oxidation due to residual oxygen in the sputtering chamber, compositional inhomogeneity, or other factors related to the deposition process. The measurements also show the evolution in the magnetic behavior as the thickness of the films increases. The thinnest sample of each P_{Ar} series presents a hysteresis curve with relative low values of coercive fields, $H_c \sim 20$–$50\,\text{Oe}$, and high remanence, in agreement with the usual behavior of in-plane planar domains. Comparatively, if we look at thicker samples, the typical features of stripe-like magnetic domains arise, such as a larger coercivity, a lower remanence due to the perpendicular component of M in the stripes, and an almost linear increase of the magnetization between $H = 0$ and the saturation field, related to the alignment of the out-of-plane component of the magnetization with the external field. The described magnetic behavior is fully consistent with the magnetic domain configuration observed by MFM in Fig. 6. For the thinner samples, planar magnetic domains are observed which change to stripe domains when the film thickness is increased

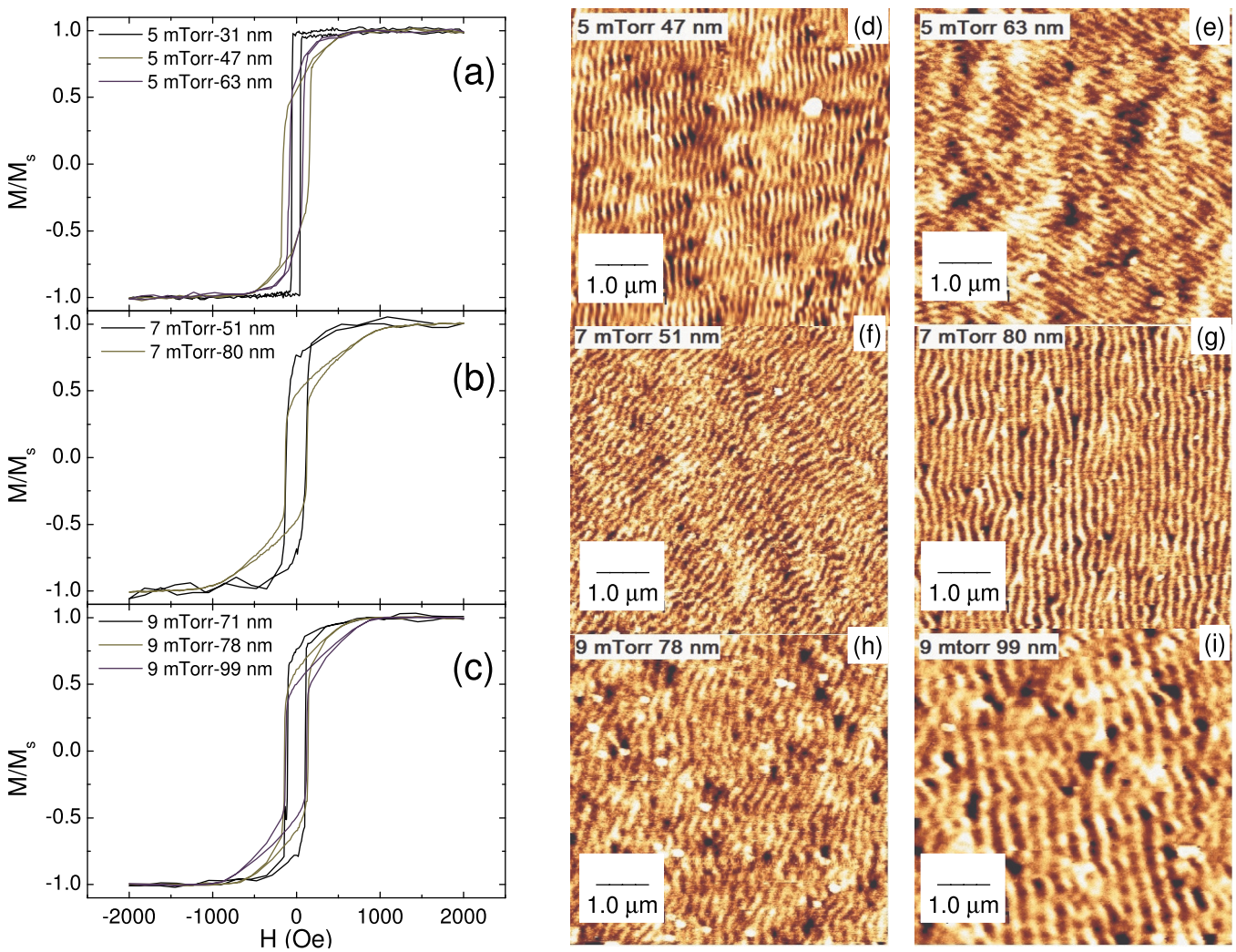

FIG. 6. Left panels (a)–(c): Hysteresis loops for representative samples of batch B, FePt/Ru grown at $P_{Ar} = 5$, 7, and 9 mTorr with the direction of the external field parallel to the plane of the films. Right panels (d)–(i): MFM images of the respective samples shown in the hysteresis loops. Image size is 5 μm × 5 μm in all cases. The images of the FePt/Ru 5 mTorr–31 nm and 9 mTorr–71 nm samples (not shown) present an in-plane magnetic domain configuration.

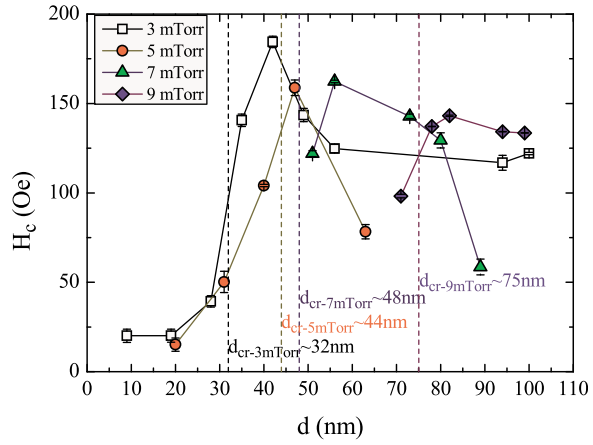

FIG. 7. Coercive field as a function of thickness for each sample of batch B. The evolution of H_c is an indication of the transition from planar to stripe domains. The vertical lines represent the estimated value of d_{cr}. For comparison, we have also added data from a series of films grown at 3 mTorr.[5]

(with the exception of $P_{Ar}=7$ mTorr for which stripes domains are already observed for $d=51$ nm).

As we discussed before, the transition between these magnetic configurations is gradual and films with thicknesses close to the critical value display some features of both systems. In Fig. 7, we can see that the coercive field H_c grows slowly for the thinner samples and then behaves as expected: it increases sharply as soon as the magnetic configuration changes to stripe-domains, due to the increasing number of the domain walls. The evolution in H_c can be taken as an indication for the change in the magnetic domain structure as a function of d. It is also possible to extract the critical thickness d_{cr} (and the half-period of the stripes, $\lambda_s/2$) using the MFM measurements shown in Fig. 6. The estimated values of d_{cr} for the different sets of films have been indicated in Fig. 7.

A simple expression of the magnetic free energy density for a thin film, which includes the interaction of the magnetization with the magnetic field and the anisotropy terms, can be written as

$$E_m = -MH\cos(\theta-\alpha) + (2\pi M_s^2 - K_\perp)\cos^2\theta, \qquad (4)$$

with $2\pi M_s^2$ the magnetostatic energy due to the thin film shape of the sample and $K_\perp$ a contribution to the perpendicular anisotropy originated by the sum of different anisotropy effects such as magnetocrystalline, stress, and surface. The angles α and θ are the angles formed by the external field and the magnetization vector from the film normal, respectively. The total effective anisotropy is usually termed as $K_{eff} = 2\pi M_s^2 - K_\perp$. Since our films have a dominant easy plane shape anisotropy, $K_{eff} > 0$. Different methods can be used to estimate the effective perpendicular anisotropy in thin films. In the frame of the Stoner-Wohlfarth model, the difference between the areas of M vs. H curves measured in the first quadrant with the external field parallel and perpendicular to the film plane is $A_{//} - A_\perp = K_{eff}$. In particular, we obtained K_{eff} from the normalized loops presented in Fig. 8. The quality factor $Q = K_\perp/(2\pi M_s^2)$ as a function of P_{Ar} was calculated from the average of the aforementioned calculations.

The perpendicular anisotropy $K_\perp$ consists essentially of magnetocrystalline and magnetoelastic contributions. An estimation of the average magnetoelastic anisotropy constant is given by $K_{me} = \frac{3}{2}\lambda\sigma_x = \frac{3}{2}\lambda E\frac{\varepsilon_x}{2\nu}$, which depends on the stress σ_x and the magnetostriction constant λ. The variable σ_x was taken as the average of both in-plane values obtained in

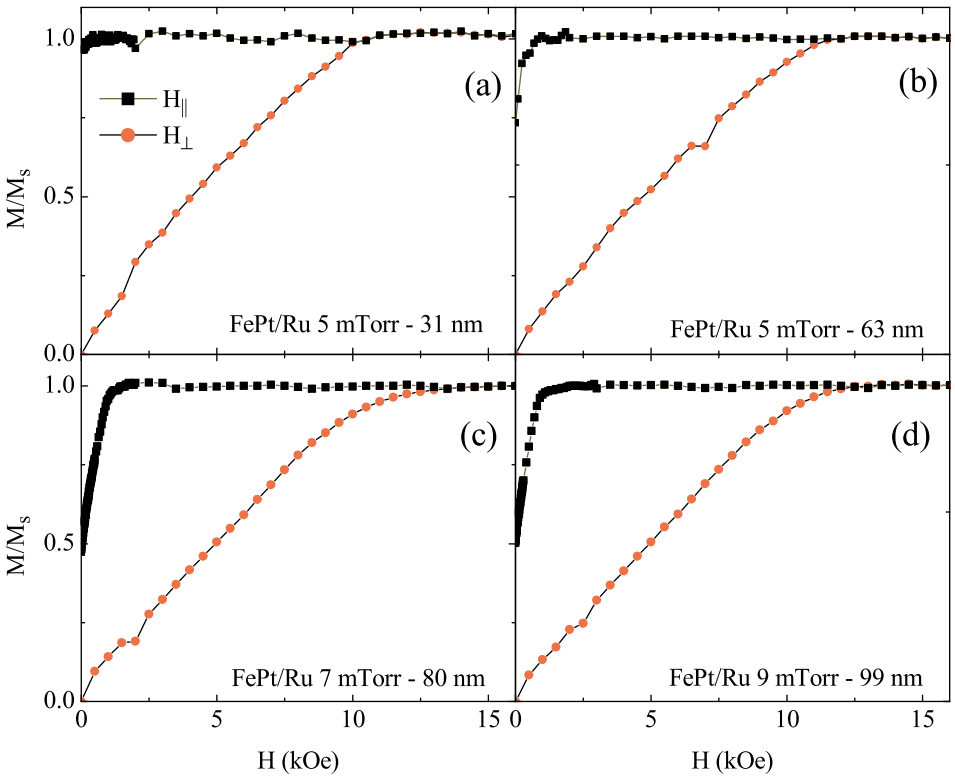

FIG. 8. First quadrant of the M vs. H curves, with H parallel and perpendicular to the film plane, for the samples FePt/Ru (a) 5 mTorr–31 nm, (b) 5 mTorr–63 nm, (c) 7 mTorr–80 nm, and (d) 9 mTorr–99 nm, all from batch B. In the Stoner-Wohlfarth model, the difference between the areas covered by both curves is $K_{eff} = 2\pi M_s^2 - K_\perp$.

Sec. III A ($\sigma_x = (\sigma_{11} + \sigma_{22})/2$), or calculated from the strain $\varepsilon_z = \frac{d_{111} - d^0_{111}}{d^0_{111}}$, estimated using the 2θ position of the (111) peak in the X-ray diffraction patterns of Fig. 1. The average magnetostriction constant λ for FePt was reported by Aboaf *et al.*,[33] $\lambda_{FePt} = 70 \times 10^{-6}$. In the disordered A1 phase, more recent measurements using differential X-ray absorption spectroscopy[34] arrived to $\lambda_{FePt-100} = 100 \times 10^{-6}$ and $\lambda_{FePt-111} = 250 \times 10^{-6}$. We used as an estimation $\langle\lambda\rangle_{FePt} = 100 \times 10^{-6}$, keeping in mind that there is a relatively large range of reported values.

In Fig. 9, we compare $K_\perp$ and K_{me} as a function of thickness for each P_{Ar}. There is a clear correlation between the overall behavior of both anisotropies, despite the relatively large error bars in the case of $K_\perp$ and the uncertainty in the absolute values of K_{me} due to the poor estimation of λ_{FePt}. The magnetoelastic anisotropy seems to be approximately independent of film thickness, except for the thicker samples of $P_{Ar} = 5$ and 7 mTorr that show a smaller value of K_{me}. This same trend also appears in $K_\perp$ (see Fig. 9(b)), although it is not so noticeable as in the former case. A possible explanation for this effect may be due to the temperature increment in the sample occurring during the sputtering process. The film temperature can rise several tens of degrees if the thermal contact is not good enough, which in turn could cause the residual stresses to relax. We would like to emphasize the similar thickness dependence of $K_\perp$ and K_{me}, showing the predominant contribution of stress effects to the perpendicular anisotropy.

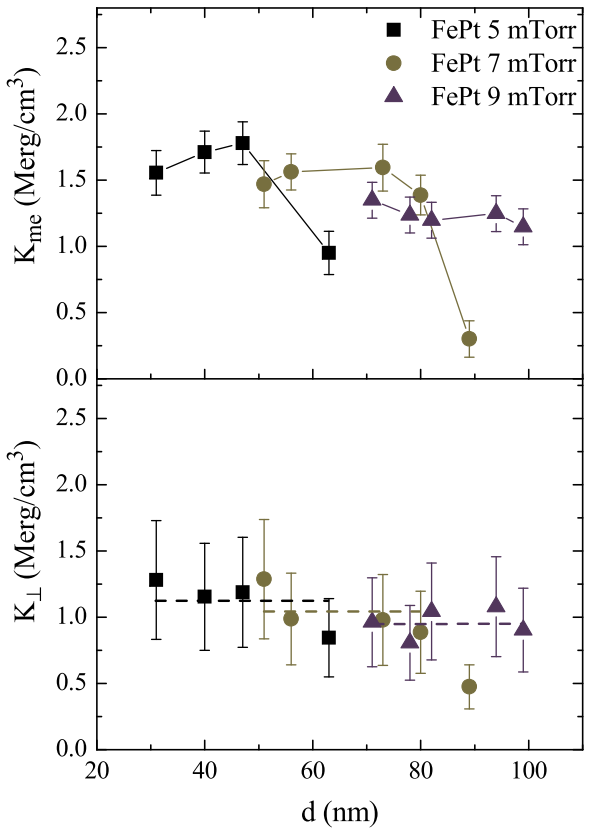

FIG. 9. Perpendicular, $K_\perp$, and magnetoelastic, K_{me}, anisotropy constants as a function of d for the samples of batch B. The values of $K_\perp$ obtained for each P_{Ar} were approximately constant (within error), for which it was assumed they were independent of the thickness. The corresponding average value for each P_{Ar} is represented by a horizontal line.

As already discussed, the analysis of the magnetic and MFM measurements allowed us to obtain a value for the critical thickness as a function of the Q-factor of each P_{Ar} batch. When $d > d_{cr}$, a stripe structure is formed which has been modeled[6,35–38] and studied experimentally[5,39–44] by various authors. In particular, our group has previously used a model proposed by Murayama[36] to describe with reasonably good results the evolution of the stripes when parameters such as thickness[5,13] or Q (Ref. 10) are varied. Murayama's model also predicts a critical curve for the transition between planar and striped magnetic domains. Sukstanskii and Primak[37] later developed a set of parametric equations linked by a single variable x (see Eqs. (5)) using a simplified model in which the magnetization distribution in the domains was homogeneous and the domain wall width was considered infinitesimally small. These assumptions were originally applied to ultrathin films, but could also be used for thicker samples

$$Q = \frac{K_\perp}{2\pi M_s^2} = \frac{1}{2\pi}\left[3x - (\pi + 3x)e^{-\pi/x}\right]$$
$$d_{cr} = d_l \frac{\sqrt{2}\pi^{3/2}}{x}\left[x - (\pi + x)e^{-\pi/x}\right]^{-1/2}. \quad (5)$$

Here, the exchange length is defined as $d_l = \frac{1}{2}\sqrt{A/2\pi M_s^2}$. In essence, this model is one-dimensional (1D-model) and assumes that the magnetization vector can only point in the direction of the stripes, alternating the out-of-plane component up and down. On the other hand, Murayama takes into account a periodic in-plane variation of the magnetization vector within the stripe structure. We have previously compared both curves,[10] finding similar results in the prediction of the critical thickness for $Q \lesssim 0.4$. In Fig. 10, we plotted the thickness of the different films studied in this work as a function of the Q–factor, distinguishing between samples in which a planar domain structure is observed (open symbols) and films in which a stripe pattern appears (full symbols).

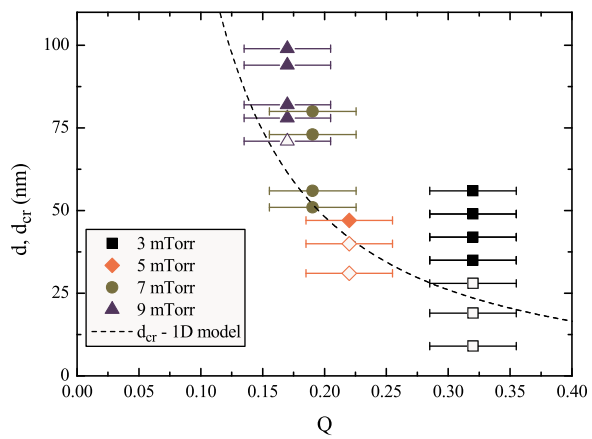

FIG. 10. Thickness as a function of the Q-factor for each P_{Ar} series (symbols) and Sukstanskii's model of d_{cr} (dashed line obtained from Eq. (5)). For each series, we assumed a constant Q value obtained from the average perpendicular anisotropy of Fig. 9. Open symbols indicate samples with in-plane magnetization, while full symbols are for samples which show stripes. Data for 3 mTorr films were taken from Ref. 5.

Note that for clarity we assumed a constant Q value for each of the $P_{Ar}=3$, 5, 7, and 9 mTorr series obtained from the average perpendicular anisotropy of Fig. 9. We have also plotted the prediction of the critical thickness as a function of Q deduced from Eq. (5). We can see that both the experimental results and the model show a decreasing $d_{cr\text{-}1D}$ for increasing Q. There is in general a reasonable good agreement between the experimental data and the values of $d_{cr\text{-}1D}$ predicted by the 1D-model for $P_{Ar}=3$, 5, 7, and 9 mTorr, giving $d_{cr\text{-}1D}$ (3mTorr)$\sim$25nm, $d_{cr\text{-}1D}$ (5mTorr)$\sim$41nm, $d_{cr\text{-}1D}$ (7mTorr) $\sim$52nm, and $d_{cr\text{-}1D}$ (9mTorr)$\sim$58nm. Small differences between data and model are observed for the $P_{Ar}=9$ mTorr batch in which the stripe pattern was only observed for the $d=78$nm sample. These differences can be accounted for by considering the uncertainty in the determination of the quality factor and the sensitivity of the $d_{cr\text{-}1D}$ model to the parameters, especially in the region of small Q. In any case, we have shown that the critical thickness for the transition between planar domains and a magnetic stripe structure can be very well controlled with the fabrication conditions (sputtering pressure) during the sputtering process, and that d_{cr} can be reasonably well predicted with existing models.

IV. CONCLUSIONS

Using different microstructural and magnetic experimental techniques, we have been able to show that the magnetic domain configuration in FePt ferromagnetic films is mainly determined by the degree of residual stresses. We also demonstrated that this variable can be effectively tuned by the Ar pressure used in the fabrication process. The dependence of the critical thickness on the Q-factor was reasonably well described by existing theoretical models, which contain no free parameters. The ability to tune the magnetic anisotropy and the domain configuration in magnetic films, together with a deep understanding of the underlying mechanisms, can be of capital importance for the design and fabrication of novel magnetoelectric devices.

ACKNOWLEDGMENTS

This work was supported in part by Conicet under Grant No. PIP 112-201101-00482, ANPCyT Grant No. PICT 2013-0401, and U. N. Cuyo Grant No. 06/C421, all from Argentina. Technical support from Rubén E. Benavides, César Pérez, and Matías Guillén is greatly acknowledged.

[1]T. Fitchorov, Y. Chen, B. Hu, S. Gillette, A. Geiler, C. Vittoria, and V. Harris, J. Appl. Phys. **110**, 123916 (2011).
[2]S. Li, H. Du, Q. Xue, X. Gao, Y. Zhang, W. Shao, T. Nan, Z. Zhou, and N. X. Sun, J. Appl. Phys. **115**, 17C723 (2014).
[3]J. Vargas and J. Gómez, APL Mater. **2**, 106105 (2014).
[4]Y. T. Yang, Y. Q. Song, D. H. Wang, J. L. Gao, L. Y. Lv, Q. Q. Cao, and Y. W. Du, J. Appl. Phys. **115**, 024903 (2014).
[5]E. Sallica Leva, R. C. Valente, F. Martínez Tabares, M. Vásquez Mansilla, S. Roshdestwensky, and A. Butera, Phys. Rev. B **82**, 144410 (2010).
[6]A. Hubert and R. Schäfer, *Magnetic Domains* (Springer, 3rd printing, 2009).
[7]S. N. Hsiao, F. T. Yuan, H. W. Chang, H. W. Huang, S. K. Chen, and H. Y. Lee, Appl. Phys. Lett. **94**, 232505 (2009).
[8]S. Tamulevičius, Vacuum **51**, 127 (1998).
[9]C. V. Thompson and R. Carel, J. Mech. Phys. Solids **44**, 657 (1996).
[10]N. R. Álvarez, M. E. Vázquez Montalbetti, J. E. Gómez, A. E. Moya Riffo, M. A. Vicente Álvarez, E. Goovaerts, and A. Butera, J. Phys. D: Appl. Phys. **48**, 405003 (2015).
[11]N. Álvarez, E. Sallica Leva, R. C. Valente, M. Vásquez Mansilla, J. Gómez, J. Milano, and A. Butera, J. Appl. Phys. **115**, 083907 (2014).
[12]M. Vásquez Mansilla, J. Gómez, E. Sallica Leva, F. Castillo Gamarra, A. Asenjo Barahona, and A. Butera, J. Magn. Magn. Mater. **321**, 2941 (2009).
[13]J. M. Guzmán, N. Álvarez, H. R. Salva, M. Vásquez Mansilla, J. Gómez, and A. Butera, J. Magn. Magn. Mater. **347**, 61 (2013).
[14]E. Burgos, E. Sallica Leva, J. Gómez, F. Martínez Tabares, M. Vásquez Mansilla, and A. Butera, Phys. Rev. B **83**, 174417 (2011).
[15]M. Vásquez Mansilla, J. Gómez, and A. Butera, IEEE Trans. Magn. **44**, 2883 (2008).
[16]N. Álvarez, G. Alejandro, J. Gómez, E. Goovaerts, and A. Butera, J. Phys. D: Appl. Phys. **46**, 505001 (2013).
[17]D. M. Jacobi, E. Sallica Leva, N. Álvarez, M. Vásquez Mansilla, J. Gómez, and A. Butera, J. Appl. Phys. **111**, 033911 (2012).
[18]R. A. McCurrie and P. Gaunt, Philos. Mag. **13**, 567 (1966).
[19]L. G. Schulz, J. Appl. Phys. **20**, 1030 (1949).
[20]D. Chateigner, P. Germi, and M. Pernet, J. Appl. Crystallogr. **25**, 766 (1992).
[21]I. Noyan and J. Cohen, *Residual Stress, Measurement by Diffraction and Interpretation* (Springer, 1987).
[22]O. Anderoglu, "Residual stress measurement using X-Ray diffraction," M.S. thesis (Texas A&M University, 2004).
[23]B. M. Clemens and J. A. Bain, MRS Bull. **17**, 46–51 (1992).
[24]P. Rasmussen, X. Rui, and J. E. Shield, Appl. Phys. Lett. **86**, 191915 (2005).
[25]F. E. Spada, F. T. Parker, C. L. Platt, and J. K. Howard, J. Appl. Phys. **94**, 5123 (2003).
[26]H. Xu, W. Zhang, B. Peng, and W. Zhang, Appl. Surf. Sci. **257**, 2689 (2011).
[27]M. Kumar, S. Mishra, and R. Mitra, Surf. Coat. Technol. **228**, 100 (2013).
[28]H.-C. Lee, G.-H. Kim, S.-K. Hong, K.-Y. Lee, Y.-J. Yong, C.-H. Chun, and J.-Y. Lee, Thin Solid Films **261**, 148 (1995).
[29]Th. Speliotis, G. Varvaro, A. M. Testa, G. Giannopoulos, E. Agostinelli, W. Li, G. Hadjipanayis, and D. Niarchos, Appl. Surf. Sci. **337**, 118 (2015).
[30]M. Ali, "Growth and study of magnetostrictive FeSiBC thin films for device applications," Ph.D. thesis (Department of Physics and Astronomy, University of Sheffield, 1999).
[31]H. J. Leamy and A. G. Dirks, J. Appl. Phys. **50**, 2871 (1979).
[32]H. Kanazawa, G. Lauhoff, and T. Suzuki, J. Appl. Phys. **87**, 6143 (2000).
[33]J. A. Aboaf, T. R. McGuire, S. R. Herd, and E. Klokholm, IEEE Trans. Magn. **20**, 1642 (1984).
[34]M. P. Ruffoni, C. B. Ndao, S. Pascarelli, and N. M. Dempsey, in Direct measurement of the local, atomic-scale, Joule magnetostriction of FePt, Joint European Magnetic Symposia, Dublin, 2008.
[35]C. Kooy and U. Enz, Philips Res. Rep. **15**, 7 (1960).
[36]Y. Murayama, J. Phys. Soc. Jpn. **21**, 2253 (1966).
[37]A. L. Sukstanskii and K. I. Primak, J. Magn. Magn. Mater. **169**, 31 (1997).
[38]R. Bručas, H. Hafermann, M. I. Katsnelson, I. L. Soroka, O. Eriksson, and B. Hjörvarsson, Phys. Rev. B **69**, 064411 (2004).
[39]N. Saito, H. Fujiwara, and Y. Sugita, J. Phys. Soc. Jpn. **19**, 421 (1964).
[40]M. Hehn, S. Padovani, K. Ounadjela, and J. P. Bucher, Phys. Rev. B **54**, 3428 (1996).
[41]V. Gehanno, R. Hoffmann, Y. Samson, A. Marty, and S. Auffret, Eur. Phys. J. B **10**, 457 (1999).
[42]S. Okamoto, N. Kikuchi, O. Kitakami, T. Miyazaki, Y. Shimada, and K. Fukamichi, Phys. Rev. B **66**, 024413 (2002).
[43]M. Barturen, B. Rache Salles, P. Schio, J. Milano, A. Butera, S. Bustingorry, C. Ramos, A. J. A. de Oliveira, M. Eddrief, E. Lacaze, F. Gendron, V. H. Etgens, and M. Marangolo, Appl. Phys. Lett. **101**, 092404 (2012).
[44]C. A. Ramos, E. Vassallo Brigneti, J. Gómez, and A. Butera, Physica B **404**, 2784 (2009).